[4]R. Gordon and G. T. Hermann, "Three-dimensional reconstruction from projections: a review of algorithms," Int. Rev. Cytol. 38, 111–151 (1974).

[5]*Technical Digest, Image Processing for 2-D and 3-D Reconstruction from Projections* (Optical Society of America, Washington, D.C., 1975).

[6]R. D. Matulka and D. J. Collins, "Determination of three-dimensional density fields from holographic interferograms," J. Appl. Phys. 42, 1109–1119 (1971).

[7]K. Iwata and R. Nagata, "Calculation of three-dimensional refractive-index distribution from interferograms," J. Opt. Soc. Am. 60, 133–135 (1970).

[8]D. W. Sweeney and C. M. Vest, "Reconstruction of three-dimensional refractive indices from multidirectional interferometric data," Appl. Opt. 12, 2649–2664 (1973).

[9]E. W. Marchand, "Derivation of the point spread function from the line spread function," J. Opt. Soc. Am. 54, 915–919 (1964); E. W. Marchand, "From line to point spread function: The general case," J. Opt. Soc. Am. 55, 352–354 (1965).

[10]J. S. Wilczynski, "Real time synthetic aperture telescope," *Synthetic Aperture Optics, Woods Hole Summer Study* (National Academy of Science, Washington, D.C., 1968), Vol. 2, pp. 183–187.

[11]K. Murata and N. Baba, "Measurement of the intensity distribution of an object by a strip telescope," Jpn. J. Appl. Phys. Suppl. 14-1, 499–503 (1975).

[12]R. M. Mersereau and A. V. Oppenheim, "Digital reconstruction of multidirectional signals from their projections," Proc. IEEE 62, 1319–1338 (1974).

[13]R. N. Bracewell and A. C. Riddle, "Inversion of fan beam scan in radio astronomy," Astrophys. J. 150, 427–434 (1967).

[14]D. A. Chesler and S. J. Riederer, "Ripple suppression during reconstruction in transverse tomography," Phys. Med. Biol. 20, 632–636 (1975).

[15]T. F. Budinger and G. T. Gullberg, "Reconstruction by two-dimensional filtering of simple superposition transverse-section image," paper ThA901, in Ref. 5.

[16]G. N. Ramachandran and A. V. Lakshminarayanan, "Three-dimensional reconstruction from radiographs and electron micrographs: II. Application of convolution instead of Fourier transforms," Proc. Nat. Acad. Sci. 68, 2236–2240 (1971).

[17]L. A. Shepp and B. F. Logan, "The Fourier reconstruction of a head section," pp. 21–43, in Ref. 3.

[18]E. Tanaka and T. A. Iinuma, "Correction functions for optimizing the reconstructed image in transverse section scan," Phys. Med. Biol. 20, 789–798 (1975).

[19]J. Sharp, J. Tiemann, and R. King, "A procedure for the synthesis of arbitrary tomographic convolution filters," paper ThA10-1, in Ref. 5.

[20]R. King, "The harmony of reconstruction: a spectral theory of X-ray tomography," paper ThA7-1, in Ref. 5.

[21]P. Jacquinot and B. Roizen-Dossier, "Apodisation," in *Progress in Optics*, edited by E. Wolf (North-Holland, Amsterdam, 1964), Vol. 3, pp. 29–186.

[22]L. S. Gruber and B. J. Thompson, "On the apodization of coherent imaging systems," Opt. Eng. 13, 451–454 (1974).

[23]R. N. Bracewell and S. J. Wernecke, "Image reconstruction over a finite field of view," J. Opt. Soc. Am. 65, 1342–1346 (1975).

[24]O. J. Tretiak, "The point-spread function for the convolutional algorithm," paper ThA5-1, in Ref. 5.

[25]P. F. C. Gilbert, "The reconstruction of a three-dimensional structure from projections and its application to electron microscopy: II. Direct methods," Proc. R. Soc. London Ser. B 182, 89–102 (1972).

[26]K. Tanabe, "Projection method for solving a singular system of linear equations and its applications," Numer. Math. 17, 203–214 (1971).

[27]T. S. Huang, D. A. Barker, and S. P. Berger, "Iterative image restoration," Appl. Opt. 14, 1165–1168 (1975).

[28]R. Gordon, R. Bender, and G. T. Hermann, "Algebraic reconstruction techniques (ART) for three-dimensional electron microscopy and x-ray photography," J. Theor. Biol. 29, 471–481 (1970).

A new proposal for estimating the spatial concentration of certain types of air pollutants

B. W. Stuck

Bell Laboratories, Murray Hill, New Jersey 07974

Electro-optical sensors measure energy transmitted by lasers spaced about a region's periphery. Both the lasers and sensors are tuned to infrared frequencies at which air pollutants strongly absorb electromagnetic energy. The sensor measurements are processed using an algorithm derived from the Radon transform. The result is an estimate of air pollutant density throughout the region that has been smoothed to minimize effects due to background sunlight fluctuations, laser fading and phase scintillation, and intrinsic sensor noise. Good agreement is found between a theoretical analysis of performance limitations and computer simulation results

I. INTRODUCTION

The inability to measure air pollution accurately and at enough points throughout an area has hindered air pollution control. A novel approach is presented here for estimating the concentration of certain types of air pollutants—those pollutants which absorb optical energy in a narrow band of optical frequencies. This approach estimates pollutant concentration at every point in a region of a plane over an area, using a network of electro-optical sensors plus lasers located about the periphery of the region. The method proposed here involves two main steps: a reconstruction of air pollutant density using linear signal processing, and spatial filtering of the reconstruction to remove effects due to noise.

The motivation for this work arose from problems with telephone switching equipment failing because of high concentrations of certain air pollutants such as nitrogen dioxide and particulates,[1,2] as well as from

problems with wire insulation degrading because of the presence of high levels of sulfur dioxide, ozone, and hydrocarbons.[3,4]

The method proposed here differs from presently used pollution monitoring schemes in several key ways. First, it provides a reliable estimate of pollution concentration at every point in a region of a plane a constant height above the ground, where the region of interest typically would encompass a highly industrialized and highly populated area, provided enough sensors and lasers are used; presently used methods typically estimate pollutant concentration at only a small number of points (e. g., 38 for New York City,[5] 22 for the state of New Jersey[6]). In fact, the method presented here may aid in the verification of the photochemistry and mass-transfer phenomena which are at the foundations of understanding air pollution. Second, the proposed method can be used to monitor several pollutants which absorb optical energy in nonoverlapping bands simultaneously; currently, different equipment is used to monitor different pollutants.[5,6] Third, all processing proposed here can be accomplished electronically, with no required intermediate processing of sensor measurements; many methods currently in use encompass a variety of wet chemical tests[5-7] whose results must often be processed further on a digital computer before the spatial distribution of various air pollutants can be estimated. Indeed it is tempting to speculate that the method proposed here would require less frequent maintenance than presently used methods, because it is largely electronic and would have fewer moving parts; however, much more work must be done in considering various important engineering design factors before it can be said with any degree of confidence that this method is more reliable.

Laser radar methods have been proposed over the past few years[8-11] which attempt to estimate particulate concentration over a region using direct backscattering of optical energy, and which estimate concentration of various chemical air pollutants over a region using both differential absorption and indirect Raman scattering of optical energy. These methods have been subjected to experimental test, and the results have been quite encouraging, with successes achieved in estimating dust particulates as well as other pollutants. Laser radar has the advantage of requiring only one laser and sensor, unlike the method presented here, which requires many lasers and sensors.

Methods closely related to that discussed here have been successfully tested in such diverse fields as radio astronomy,[12] medical x-ray photography[13] (in particular with an eye toward identifying brain tumors),[14,15] and industrial x-ray photography,[16] and it is reasonable to expect the number of applications to grow. In order to interest experimentalists in this approach, as well as to alert them to possible pitfalls, an extensive computer simulation has been carried out. A hypothetical air pollutant distribution was successfully reconstructed both with and without additive Gaussian noise present in the sensor measurements. Results of the simulation were in good agreement with a theoretical analysis. A

key conclusion of this work is that qualitative estimates of the spatial distribution of air pollution can be obtained from four or five (or in special cases as few as two) lasers and sensors, but quantitative estimates with a root-mean-square absolute error of 5% or less (see Table II) require at least 20 sensors and lasers. In addition, the simulation showed that the technique is relatively insensitive to gross measurement imperfections. The chief advantage this method has over laser radar methods is that it uses energy absorption bands of the pollutants, which is a high "signal-to-noise ratio" technique, while laser radar relies on backscattered energy, which can be a low "signal-to-noise ratio" technique.

A number of people have proposed using differential absorption spectroscopy to measure air pollutants.[17-24] The results to date appear quite promising and may soon be used by government agencies to provide air quality information on a routine daily basis. The method proposed here, at the expense of a more complicated measurement system, provides an accurate estimate of air pollution density at every point in a region of a plane by a totally different method than laser radar. These more accurate estimates can then be used to determine more effective air pollution control methods than those currently in use.

This paper follows very closely earlier work by Shepp and Logan[14,15] for detecting brain tumors from x-ray measurements. Their contribution is cited at the appropriate place.

The following section states the problem to be addressed, presents several approximate solutions, and delves into some theoretical limitations of these solutions. A hypothetical air pollution distribution is used in Sec. III as a test of how well one particularly attractive solution performs; theoretical predictions and computer simulation results are found to be in good agreement. In Sec. IV effects of additive Gaussian noise on the reconstruction are examined both theoretically and with Monte Carlo computer simulations, and a scheme for reducing effects due to noise is shown to perform well; in addition, various effects due to measurement imperfections are found from simulations to be negligible.

II. PROBLEM STATEMENT

A laser located at point A transmits a constant signal of power P_T, with energy confined to a narrow band of optical frequencies to a receiver at point B for a known fixed time interval. A phenomenological theory of radiation transport, the theory of radiative transfer,[25] is assumed to adequately model atmospheric light propagation. This theory shows the received power P_R detected at the receiver with regard to coordinates (x, y, z) is

$$P_R = P_T \exp\left(-K \int_A^B f(x, y, z)\, ds\right) \overline{\exp(n)}, \qquad (2.1)$$

where the overbar denotes expectation: $\overline{e^n} = \int e^n p(n)\, dn$, with $p(n)$ the probability density of n; $f(x, y, z)$ is the (dimensionless) spatial density of a substance which ab-

sorbs optical energy in the transmitted band of optical frequencies, K is a scaling or calibration constant which is known *a priori*, and n arises from background sunlight fluctuations, laser fading, and phase scintillation,[26] and intrinsic sensor noise.[27] Recent theoretical work[28,29] has indicated that radiative transfer theory adequately models light propagation as long as the optical path length is much less than unity, which means that

$$K \int_A^B f(x, y, z)\,ds \ll 1 \qquad (2.2)$$

is assumed to hold. For this reason, this presently restricts the path lengths over which (2.1) can be expected to hold to 10 km or less.

Table I lists some common air pollutants, some wavelengths at which these pollutants strongly absorb optical energy, and typical absorption coefficients which were measured in a laboratory by transmitting a laser with a known power through a known (assumed uniform) concentration of a pollutant for a fixed distance, comparing received and transmitted power levels.[19]

We chose coordinates such that the z axis points upward from a plane parallel to the ground, with the x and y axes forming a plane parallel to the earth (neglecting curvature). In order to restrict the scope of the problem, it is assumed that an estimate of pollutant concentration is desired in a region of a plane, a plane being a constant height above ground ($z = z_0 = $ constant); thus only a two-dimensional cross section of the three-dimensional pollutant distribution is desired.

For mathematical convenience, assume the region of the plane is a circle of unit radius, so that outside the circle the pollution concentration is assumed to be zero:

$$f(x, y, z_0) = 0 \qquad x^2 + y^2 > 1 \ . \qquad (2.3)$$

Finally, for the time being, effects due to uncertainty

TABLE I. Gas absorption coefficients.[a]

Gas	Absorption Wavelength (μm)	K(cm^{-1}/ppm)
CO	4.74	1×10^{-5}
O_3	4.75	5×10^{-6}
NO	5.31	1×10^{-5}
SO_2	8.88	1×10^{-6}
C_2H_4	10.54	2×10^{-5}

(1) NO_2 has an absorption coefficient one-third that of NO at 5.31 μm. In order to estimate the amount of each species, measurements must be performed at another frequency. See last section for some additional comments. (Source: unpublished work performed at Bell Laboratories.)

(2) Absorption due to water vapor is negligible at these frequencies (Source: unpublished work performed at Bell Laboratories.)

(3) NO_2, PAN, and other chemical species have been ignored here, although they do contribute significantly to air pollution.

are ignored, with n in (2.1) set to zero. The problem is as follows: Given a set of measurements of received power over as many paths as desired,

$$P_R(A, B) = P_T \exp\left(-K \int_A^B f(x, y, z_0)\,ds\right), \qquad (2.4a)$$

or, equivalently, given the logarithm of received power to transmitted power, over as many paths as desired,

$$\ln[P_R(A, B)/P_T] = -K \int_A^B f(x, y, z_0)\,ds \ , \qquad (2.4b)$$

then reconstruct or estimate $f(x, y, z_0)$ from this data. Clearly this is impossible unless the paths cover the unit circle sufficiently densely. Section IIA shows how to reconstruct $f(x, y, z_0)$ from this data given *all* straight lines that cover the unit circle, while Sec. IIB presents some good reconstruction algorithms given only a finite number of measurements, which is more realistic. The problem of finding a best or optimal reconstruction from only a finite number of measurements for any reasonable optimality criterion is still open.[30]

A. A Fourier reconstruction scheme

In this section, $f(x, y)$ is assumed to be square integrable over the unit circle, so that its Fourier transform exists. Let $\tilde{f}(r, \varphi)$ be the line integral [$\tilde{f}(r, \varphi)$ is called the Radon transform[31] of $f(x, y)$] of $f(x, y)$ along a line a distance r from the origin making an angle φ with the y axis. This line integral can be written

$$\tilde{f}(r, \varphi) = \int f(x, y)\,ds$$

$$= \int_{-\infty}^{\infty} \int_{-\infty}^{\infty} f(x, y)\delta(r - x \cos\varphi - y \sin\varphi)\,dx\,dy \ , \qquad (2.5)$$

where $\delta(\cdots)$ is a Dirac delta function. It is important in the later development to realize

$$\tilde{f}(r, \varphi) = \tilde{f}(-r, \varphi + \pi) \ , \qquad (2.6)$$

which follows from (2.5) and is clear on physical grounds. The Fourier transform of $f(x, y)$ is $\bar{f}(a, b)$, where

$$\bar{f}(a, b) = \int_{-\infty}^{\infty} \int_{-\infty}^{\infty} f(x, y)\varphi^{-i2\pi(ax+by)}\,dx\,dy \ , \qquad (2.7)$$

which can be rewritten in polar frequency coordinates as

$$\hat{f}(a = R \cos\theta, b = R \sin\theta) = \hat{f}(R, \theta) \ , \qquad (2.8)$$

$$\hat{f}(R, \theta) = \int_{-\infty}^{\infty} \int_{-\infty}^{\infty} f(x, y) \exp[-i2\pi R(x \cos\theta + y \sin\theta)]\,dx\,dy \ . \qquad (2.9)$$

On the other hand, the Fourier transform $\hat{f}(R, \theta)$ and the line integral $\tilde{f}(r, \varphi)$ can be shown to form a transform pair:

$$\tilde{f}(r, \varphi) = \int_{-\infty}^{\infty} \hat{f}(R, \varphi) e^{i2\pi Rr}\,dR \ , \qquad (2.10)$$

$$\hat{f}(R, \theta) = \int_{-\infty}^{\infty} \tilde{f}(r, \theta) e^{-i2\pi Rr}\,dr \ . \qquad (2.11)$$

This fact can be used to express $f(x, y)$ as the inverse Fourier transform of the Fourier transform of its line integral:

$$f(x,y) = \int_0^{2\pi} d\theta \int_0^\infty \left(\int_{-\infty}^\infty \tilde{f}(r,\theta) e^{-i2\pi Rr} \, dr \right)$$
$$\times \exp[i2\pi R(x\cos\theta + y\sin\theta)] R \, dR \quad . \qquad (2.12)$$

This can be used in conjunction with (2.6) to show

$$f(x,y) = \int_0^{2\pi} d\theta \int_{-\infty}^\infty \int_{-\infty}^\infty \frac{|R|}{2} \tilde{f}(r,\theta)$$
$$\times \exp[i2\pi R(x\cos\theta + y\sin\theta - r)] \, dr \, dR \quad . \qquad (2.13)$$

This last expression can be recognized as computing one-half the derivative of the Hilbert transform of $\tilde{f}(r,\theta)$, then integrating over θ, because $|R| = (iR)(-i\,\mathrm{sgn}R)$ is the product of the (generalized) Fourier transforms of differentiation (iR) and Hilbert transformation $(-i\,\mathrm{sgn}R)$.

This exercise implicitly assumes the line integrals $\tilde{f}(r,\varphi)$ are known for all lines covering the unit circle. Section IIB examines the important practical case where only a finite number of line integrals are known.

Three examples of $\tilde{f}(r,\varphi)$ for some analytically tractable functions complete this section.

Example 1 (disc):

$$f(x,y) = \begin{cases} 1, & x^2 + y^2 < R^2 \\ 0, & x^2 + y^2 > R^2 \end{cases}$$

$$\tilde{f}(r,\varphi) = \int f(x,y) \, ds = \begin{cases} 2(R^2 - r^2)^{1/2}, & r < R \\ 0, & r > R \end{cases}$$

Example 2 (ellipse):

$$f(x,y) = \begin{cases} 1, & \left(\dfrac{x}{a}\right)^2 + \left(\dfrac{y}{b}\right)^2 < \dfrac{1}{c^2} \\ 0, & \left(\dfrac{x}{a}\right)^2 + \left(\dfrac{y}{b}\right)^2 > \dfrac{1}{c^2} \end{cases}$$

$$\tilde{f}(r,\varphi) = \begin{cases} 2ab[(s/c)^2 - r^2]^{1/2}/s^2, & s/c > r \\ 0, & s/c < r \end{cases}$$

where

$$s^2 = (b\sin\varphi)^2 + (a\cos\varphi)^2 \quad .$$

Example 3 (Gaussian):

$$f(x,y) = \frac{1}{2\pi ab} \exp\left\{ -\frac{1}{2}\left[\left(\frac{x}{a}\right)^2 + \left(\frac{y}{b}\right)^2 \right] \right\} \quad ,$$

$$\tilde{f}(r,\varphi) = 1/\sqrt{2\pi}S \, e^{-r^2/2s^2},$$

$$S^2 = (b\cos\varphi)^2 + (a\sin\varphi)^2 \quad .$$

[Note: The last example violates the assumption that $f(x,y)$ is zero outside a unit circle centered at the origin, but it can be handled using a different technical condition with little difficulty.]

B. Some approximate reconstruction techniques

Two avenues are open for approximately reconstructing $f(x,y)$ from only a finite number of measurements: One involves approximating (2.13), while the other involves expressing (2.13) as a convolution, i.e.,

$$f(x,y) = \int_0^{2\pi} d\theta \int_{-\infty}^\infty \tilde{f}(r,\theta) w(x\cos\theta + y\sin\theta - r) \, dr \quad , \qquad (2.14)$$

where $w(\cdots)$ is a weighting function whose Fourier transform approximates that given in (2.13). Note that $w(\cdots)$ weights line integrals according to how far the point (x,y) is from the line over which $\tilde{f}$ was evaluated. In either approach, the key approximation is to choose a weighting function whose Fourier transform is approximately $|R|/2$ for low frequencies ($|R| \ll 1$) and goes to zero at high frequencies ($|R| \gg 1$).

A reasonable approximation at first sight might be to use two discrete fast Fourier transforms to approximate (2.13), in conjunction with some recently developed discrete approximations to differentiation and Hilbert transforms.[32,33] This approach has been examined in detail elsewhere.[34] Shepp and Logan[14,15] have argued that this approach may take longer to compute than a direct approximation of the convolution integral in (2.14); since these arguments are quite cogent, the rest of this section is devoted to approximating $f(x,y)$ via convolutions.

If $\tilde{f}(r,\theta)$ is known for only evenly spaced values of r and θ, at

$$r = r_j = jd, \qquad j = 0, \pm 1, \pm 2, \ldots \qquad (2.15a)$$

$$\theta = \theta_k = k\pi/N, \qquad k = 0, 1, \ldots, N-1 \qquad (2.15b)$$

then (2.14) can be approximated as

$$f_w(x,y) = \frac{2d\pi}{N} \sum_{k=0}^{N-1} \sum_{j=-\infty}^\infty \tilde{f}(r_j, \theta_k) w(x\cos\theta_k + y\sin\theta_k - r_j) \quad , \qquad (2.16)$$

where to emphasize the estimate of f depends on the weighting function w, the estimate is denoted f_w. Since f is zero by assumption outside a unit radius circle, the inner sum in (2.16) has only a finite number of terms, but it is convenient to leave the summation limits infinite. Line integrals are only necessary for $0 \le \theta \le \pi$, since these integrals are identical to those of $\pi \le \theta \le 2\pi$ from (2.6) and on physical grounds.

One method for choosing a weighting function is to examine

$$w_B(R) = \int_{-B}^B \frac{1}{2}|f| \, e^{i2\pi fR} \, df \quad , \qquad (2.17)$$

which is a band-limited approximation to the ideal weighting function[12]; this function can be expressed

$$w_B(R) = \frac{B^2}{2}\left[2\left(\frac{\sin 2\pi BR}{2\pi BR}\right) - \left(\frac{\sin \pi BR}{\pi BR}\right)^2 \right] \qquad (2.18)$$

and used in (2.16). It can be shown that a much simpler weighting pattern than (2.18) achieves virtually the same error as this scheme but at a much cheaper computation cost, which is important in applications.[14,15]

Ramachandran and Lakshminarayanan[13] considered weighting functions which are specified only at evenly spaced points,

$$\{w(jd); \quad j = 0, \pm 1, \pm 2, \pm 3, \ldots\} \quad , \qquad (2.19)$$

and are linear between these points. The Fourier transform of a typical member from this class of weighting

functions is

$$\hat{w}(t) = d \left(\frac{\sin \pi dt}{\pi dt} \right)^2 \sum_{j=-\infty}^{\infty} w(jd) e^{i2\pi tjd} , \qquad (2.20)$$

$$\hat{w}(t) \triangleq d \left(\frac{\sin \pi dt}{\pi dt} \right)^2 \tilde{w}(t) . \qquad (2.21)$$

Choosing the weights $\{w(jd)\}$ such that for low frequencies $\tilde{w}(t)$ is proportional to $|t|$ can be shown to yield a weighting function that will accurately estimate f as long as f has negligible energy at high frequencies. The reason for considering this class of weighting functions is that the inner sum in (2.16) can be computed once for each angle, and linearly interpolated at points in between whenever necessary [which will be at points where $(x \cos\theta_k + y \sin\theta_k - r_j) \ne jd]$. This simple observation is what achieves a great increase in computation speed over (2.18).

One possible choice of weights is

$$w(0) = 1/8d^2 , \qquad (2.22a)$$

$$w(jd) = w(-jd) = -4w(0)/\pi^2 j^2, \quad j = \pm 1, \pm 3, \pm 5, \dots \qquad (2.22b)$$

$$w(jd) = w(-jd) = 0, \quad j = \pm 2, \pm 4, \pm 6, \dots \qquad (2.22c)$$

which corresponds to sampling (2.18) at evenly spaced points.

A second possible choice is

$$w(0) = 1/\pi^2 d^2 , \qquad (2.23a)$$

$$w(jd) = w(-jd) = -w(0)/(4j^2 - 1), \quad j = \pm 1, \pm 2, \pm 3, \dots \qquad (2.23b)$$

which corresponds to choosing $\tilde{w}(t) = |\sin \pi dt|/2\pi d^2$. Note that both these weighting functions weight data on either side of the $j = 0$ line negatively; (2.22) oscillates from zero to a negative number as j goes from one to infinity, while (2.23) is monotone decreasing and negative over the same range.

The reader should realize that given only a finite number of evenly spaced line integrals of f [(2.14)–(2.15)], there exist infinitely many highly oscillatory nonzero functions that have a zero line integral in each of the given directions. This is because no assumptions were made about the smoothness of f, loosely speaking.

C. Another approach

One disadvantage of the convolution approach is there is no guarantee that the projections of the reconstructed function are close to the actual line integral measurements. Several other algorithms have been proposed to overcome this shortcoming, using various iterative search algorithms.[35,36] In a forthcoming paper by the author, computer simulation results for the convolution approach and a search algorithm are compared in detail. A representative result is the following: to reconstruct f at a grid of 60×60 points with ten lasers and ten sensors via the convolution approach took 40 s on a Honeywell 6070 computer with a root-mean-square absolute error (see Table II) of 53.7%; the same problem on the same computer using an iterative search algorithm took 20 s per iteration and required ten iterations to achieve a root-mean-square error of 66.1%. In addition, this algorithm was more sensitive to noise than the convolution approach, based on simulation results. Shepp and Logan[14,15] have also studied this problem and concluded that the search algorithm is much slower and hence more expensive in computation time than the convolution approach.

III. PERFORMANCE WITHOUT NOISE PRESENT

Two methods are used in this section to assess the performance of the convolution approach: one method studies how well a particular weighting function reconstructs a delta function, while the second examines how accurately a particular weighting function reconstructs various representative functions.
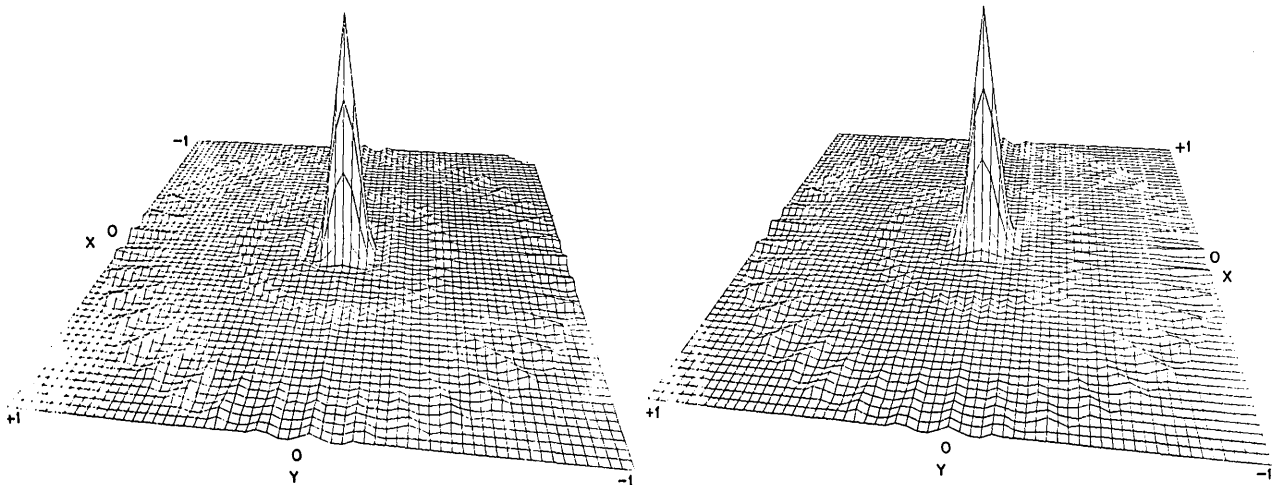

FIG. 1. Left: reconstruction of a delta function at a 60×60 grid of points using piecewise linear approximation (2.22) to Bracewell-Riddle (Ref. 12) weighting function; 20 lasers and 20 sensors were used. Right: same as left except piecewise linear approximation (2.23) suggested by Shepp and Logan (Refs. 14 and 15) was used.

TABLE II. Estimated error in reconstructing an impulse using Eq. (2.16).

$$e_{ij} = e(x_i, y_j) = |f(x_i, y_j) - f_w(x_i, y_j)|, \quad i = 1, \ldots, N_x, \; j = 1, \ldots, N_y, \; N_x = 60, \; N_y = 60$$

$$E_1 \triangleq \frac{1}{N_x N_y} \sum_{i=1}^{N_x} \sum_{j=1}^{N_y} e_{ij} ,$$

$$E_2^2 \triangleq \frac{1}{N_x N_y} \sum_{i=1}^{N_x} \sum_{j=1}^{N_y} e_{ij}^2 ,$$

$$E_\infty \triangleq \max_{\substack{i=1\ldots N_x \\ j=1\ldots N_y}} e_{ij} .$$

Number of lasers and sensors	w in (2.22)			w in (2.23)		
	E_1	E_2	E_∞	E_1	E_2	E_∞
2	0.284	0.407	1.00	0.283	0.416	1.00
4	0.117	0.173	0.595	0.116	0.179	0.656
6	0.0471	0.110	0.613	0.468	0.116	0.669
8	0.0294	0.0831	0.603	0.0278	0.0870	0.662
10	0.0206	0.0683	0.651	0.0193	0.0724	0.684
20	0.00711	0.0336	0.554	0.00606	0.0323	0.615

A. Impulse response

One approach to characterizing weighting patterns is to compare how well a given weighting function reconstructs a delta function with regard to number and amplitude of oscillations in the reconstruction.

Figure 1 (left) shows a reconstruction of a delta function at $x = y = 0$ using the weighting function in (2.22). For comparison, Fig. 1 (right) shows a reconstruction of the same delta function using (2.23) for weights. Table II presents various error estimates as a function of the number of sensors and lasers.

It can be shown that approximating $f(x, y)$ by $f_w(x, y)$ in (2.16) is equivalent to integrating $f(x, y)$ weighted by a triangular smoothing kernel over a strip of width equal to the radial spacing between measurements, then smoothing the strip integrals with the inverse Fourier

transform of $\tilde{w}(t)$. This suggests that examining the impulse response of various weighting functions will not give enough information to choose one weighting function over another, a suspicion born out by Fig. 1 and Table II.

B. An example

Figure 2 is a three-dimensional perspective plot of what is felt to be a representative distribution of a particular air pollutant, which the reader can take to be sulfur dioxide for concreteness. The function is a superposition of three homogeneous ellipses of differing densities. Table III is a list of the parameters describing this function. Results virtually identical to those to be presented were obtained where the ellipses were replaced by Gaussian functions with the same major and minor axes, orientations, and densities. A very rich class of functions can be obtained from superposition of ellipses.

How well does this function represent the spatial distribution of an arbitrary air pollutant? From private communications with people presently active in analyzing air pollution data,[5-7] it appears that the distribution of pollutants such as ozone may not be nearly as localized as the example shown here, while the distribution of pollutants such as carbon monoxide may be concentrated into patches smaller than those in the figure. Thus this example was chosen to fall midway between these extremes, in order to bring out the merits and demerits of the approach presented here for estimating the spatial distribution of a variety of pollutants. All three ellipses (in particular III) are quite small in size compared with the distance between the lines along which $f(x, y)$ is integrated, making this a difficult (but hopefully realistic) problem.
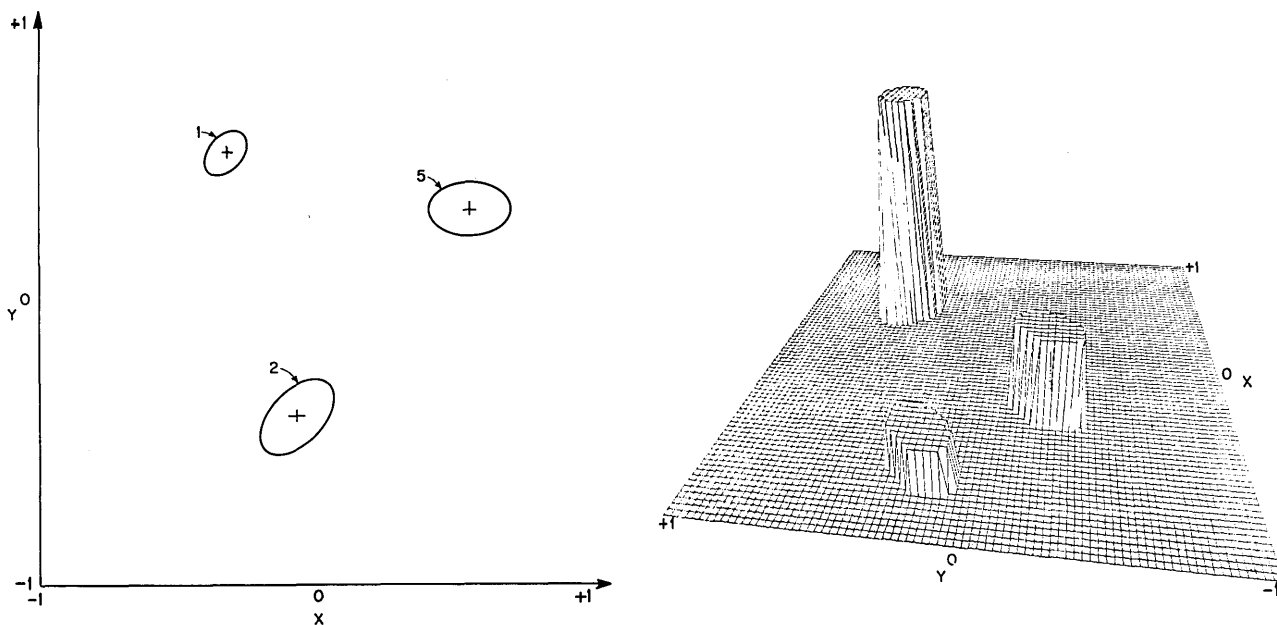

FIG. 2. Hypothetical air pollutant distribution; $f(x, y)$ is a superposition of three ellipses. Left: contour plot of $f(x, y)$. Right: three-dimensional perspective plot. (The sloping lines at the edges of the ellipses are due to linear interpolation in the plotting computer routine.)
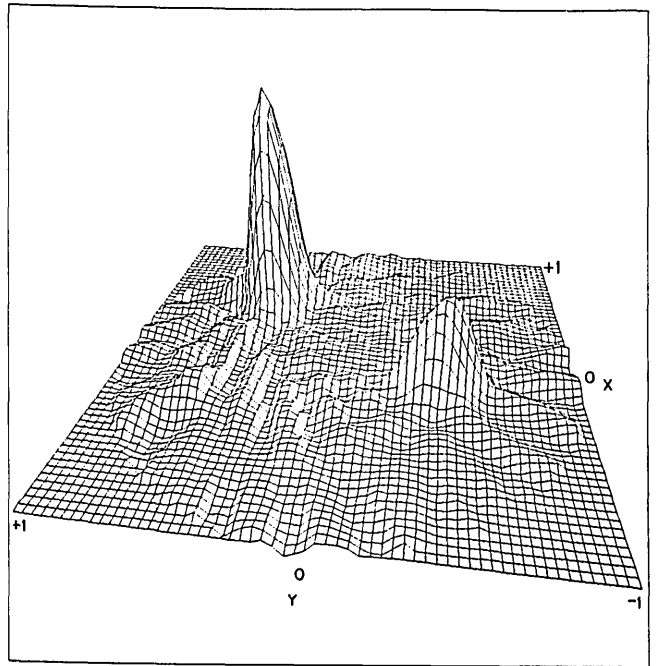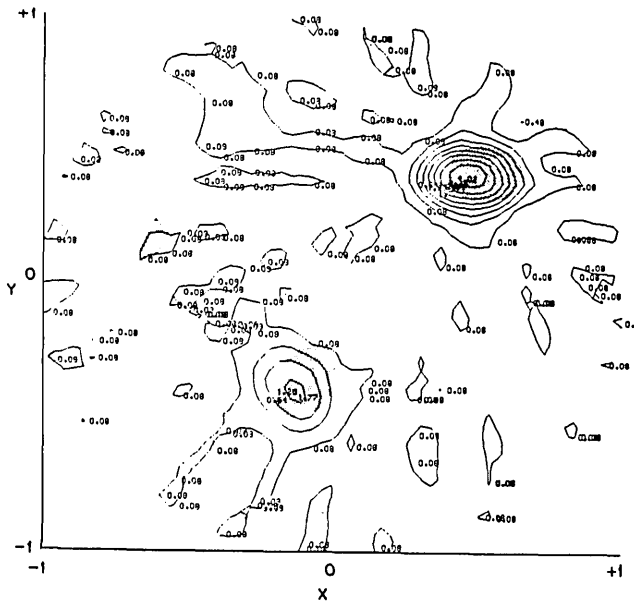
FIG. 3. Reconstruction of $f(x, y)$ at 60×60 grid of points using (2.23) as a weighting pattern with 20 lasers and 20 sensors. Reconstruction is truncated outside unit disk. Left: contour plot, with actual ellipses shaded in crosshatch. Right: three-dimensional perspective plot.

Figure 3 is a reconstruction of the function using 20 lasers and sensors at a 60×60 grid of points in the x-y plane using (2.22) for a weighting function; Fig. 4 is identical except that (2.23) has been used to weight the line integrals.

The third or bottom ellipse clearly evident in Fig. 2 is obscured in Figs. 3 and 4 partly by inaccuracies in

reconstructing the function and partly by distortions inherent in three-dimensional perspective plots.

The distortion evident at the edges of Figs. 3 and 4 (as well as Fig. 5) is probably intrinsic to the convolution approach. An explanation for this curious (and difficult) phenomenon has been advanced elsewhere. [15]

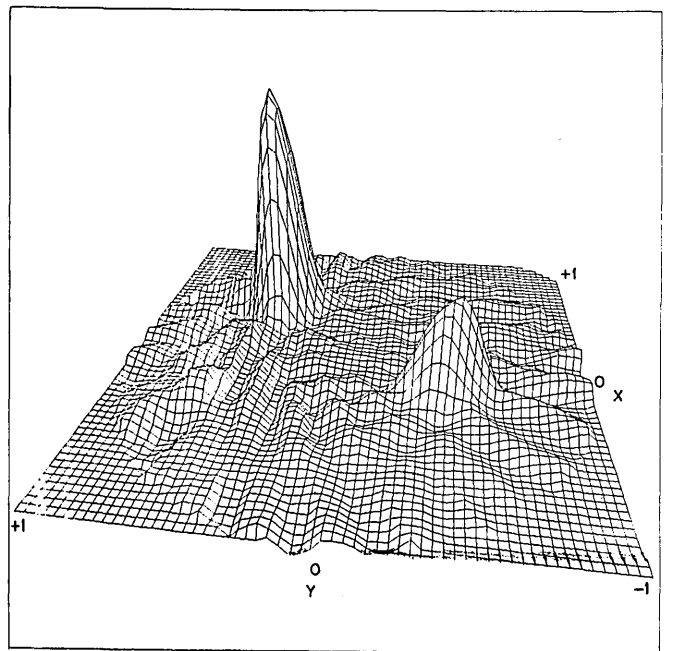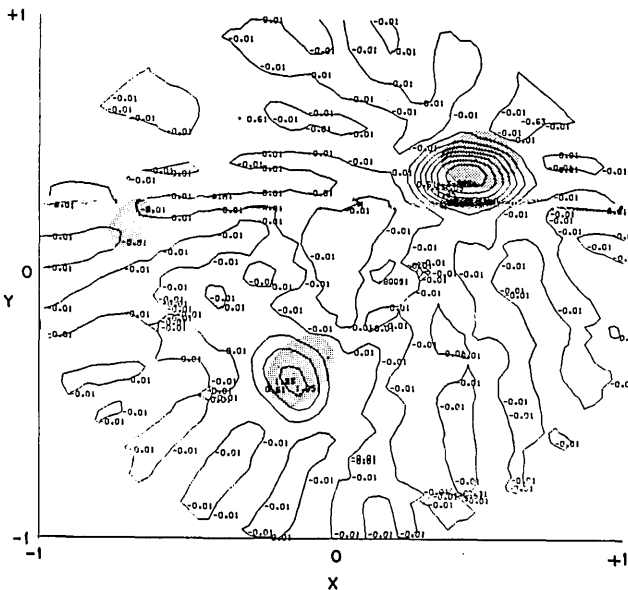The important practical issue of how few lasers and

FIG. 4. Reconstruction of $f(x, y)$ at 60×60 grid of points using (2.22) as a weighting pattern with 20 lasers and 20 sensors. Reconstruction is truncated outside unit disk. Left: contour plot, with actual ellipses shaded in crosshatch. Right: three-dimensional perspective plot.
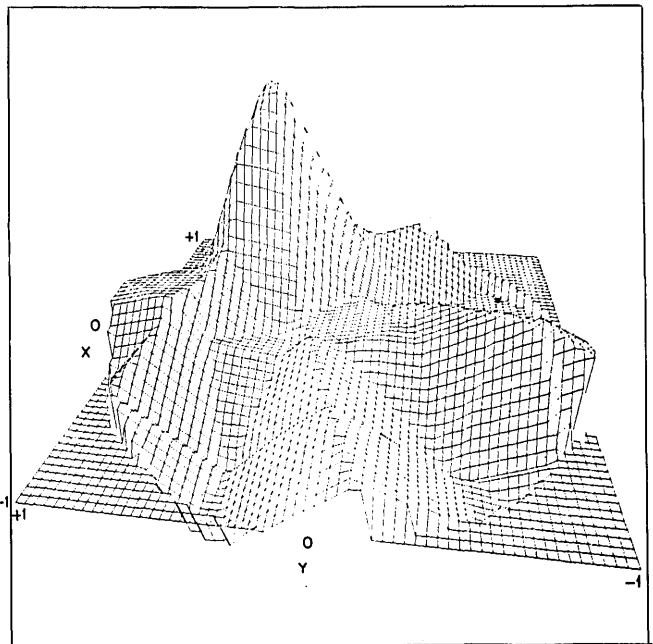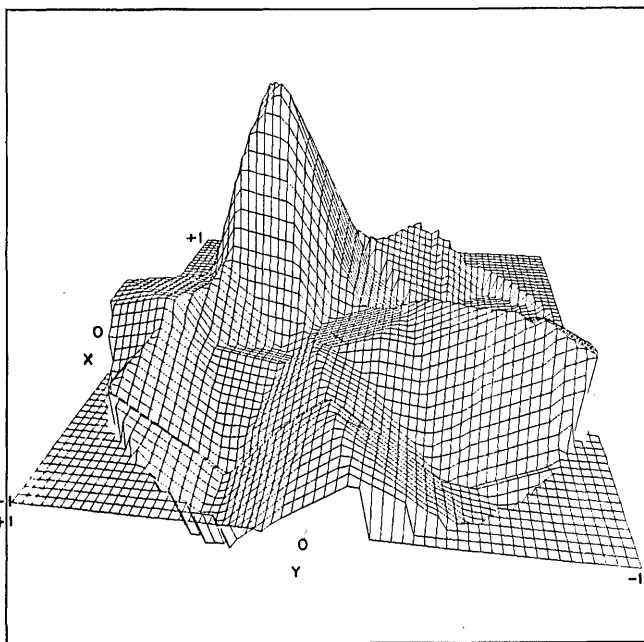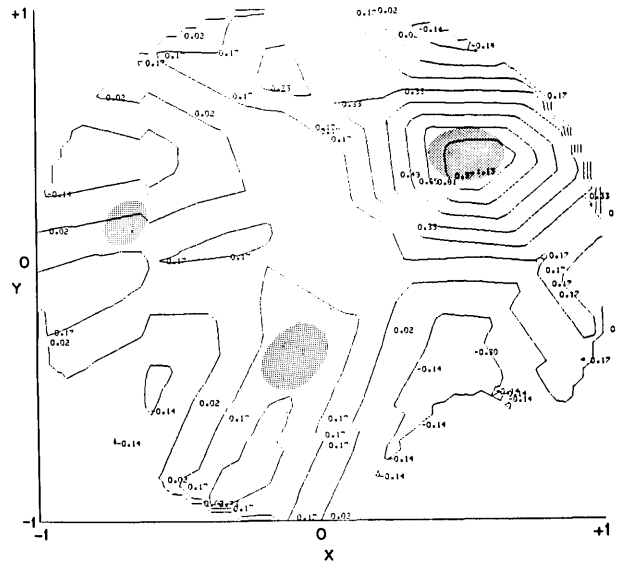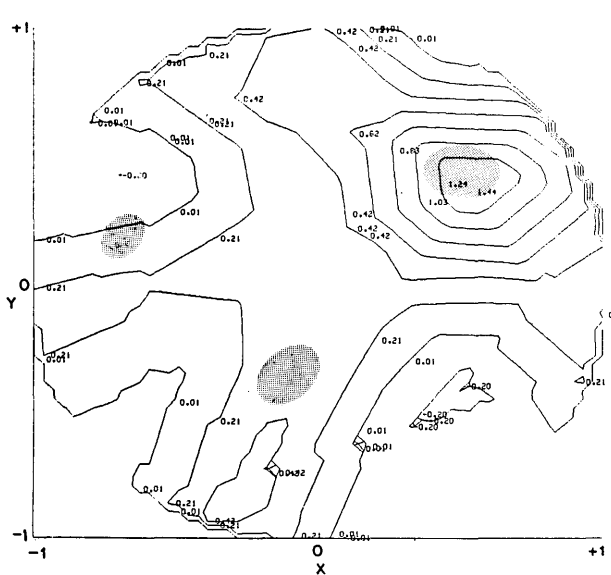
FIG. 5. Reconstruction of $f(x, y)$ at 60×60 grid of points using (2.22) as a weighting pattern with five lasers and five sensors (left, top, and bottom) and with five lasers and five sensors using (2.23) (right, top and bottom).

sensors are needed to accurately estimate $f(x, y)$ is now considered. This point has been largely ignored in any other work on this topic, and is considered in much greater detail in a forthcoming paper by the author. Figure 5 (left) is a reconstruction using five lasers and sensors, weighting the measurements as in (2.23), but otherwise identical to Fig. 3. Figure 5 (right) is a reconstruction using five lasers and sensors but in all other respects the same as Fig. 4. It is clear that some qualitative information can be obtained from Fig. 5 concerning gross pollution distribution, but Figs. 3 or 4 are a more accurate reconstruction. Based on this as well as on much more evidence not presented here, it is concluded that some qualitative information concerning pollution distribution can be obtained with five lasers and sensors, but in order to achieve estimates of $f(x, y)$ accurate to within a root-mean-square absolute error of 50% or less, at least ten lasers and sensors must be used. Table IV below is a sampling of various error estimates in reconstructing $f(x, y)$ as a function of number of lasers and sensors.

IV. EFFECTS OF UNCERTAINTY

In this section effects due to uncertainty in sensor measurements caused by background sunlight fluctuations, laser fading and phase scintillation, and intrinsic sensor noise are examined. If we choose a different

TABLE III. Parameters describing $f(x, y)$.

Ellipse	Center	Major axis	Minor axis	Orientation	Density
I	$x_0 = -0.123$ $y_0 = -0.370$	0.15	0.10	$(\pi/6)$	2
II	$x_0 = 0.424$ $y_0 = 0.424$	0.15	0.10	(0)	5
III	$x_0 = -0.350$ $y_0 = 0.607$	1.10	0.05	$(-\pi/4)$	1

(but related) weighting function to that in (2.19), these effects can be reduced at the expense of accuracy, but not enough to limit potential usefulness. The analysis presented here is only a first attempt.

A. Theoretical analysis of effects of noise

Since the average transmitted power (P_T) and received power (P_R) are directly proportional to the average number of transmitted photons $(\bar{N}_T)$ and detected photons $(\bar{N}_D)$, (2.1) can be rewritten (heuristically) as

$$N_D = \exp\left[-K \int_L f(x, y) \, ds\right] e^n E N_T , \qquad (4.1)$$

where E is the efficiency of the detector (assumed to be unity), and n is a Gaussian random process with mean m and variance σ^2 which models background sunlight fluctuations, laser fading and phase scintillation,[21] and intrinsic sensor noise.[22]

The following simplifying assumptions are now introduced: (i) N_D and N_T, which are Poisson distributed, can be approximated as Gaussian random variables with means $\bar{N}_D$ and $\bar{N}_T$ and variances $\bar{N}_D$ and $\bar{N}_T$, respectively $(\bar{N}_D \gg 1, \bar{N}_T \gg 1)$, $N_D \cong \bar{N}_D[1 + n'/(\bar{N}_D)^{1/2}]$; (ii) $\ln(1 + x) \doteq x$, $|x| \ll 1$; and (iii) $\bar{N}_T \gg \bar{N}_D$.[26] This can be used to rewrite (4.1)

$$\ln(N_D/N_T) \doteq \ln(\bar{N}_D/\bar{N}_T) + n'/(\bar{N}_D)^{1/2}$$

$$= -K \int f(x, y) \, ds + \ln E + n , \qquad (4.2)$$

where n' is Gaussian with zero mean and unit variance. Clearly this assumes the fluctuation in N_T is negligible compared with laser fading and background sunlight fluctuations.

The proceeding suggests that as a first cut the measurements in (2.16) are related to the physics as follows:

$$\bar{f}(r_j, \theta_k) = \bar{f}(r_j, \theta_k) + \sigma_{kj} n(r_j, \theta_k), \quad j = 0, \pm 1, \pm 2, \dots \quad (4.3)$$

$$\bar{f}(r_j, \theta_k) = \ln(\bar{N}_D/\bar{N}_T) \sigma_{kj}^2 = 1/\bar{N}_D, \quad k = 0, 1, \dots, N-1$$

with each measurement having mean $\bar{f}$ and variance σ_{kj}^2, and $n(r_j, \theta_k)$ is a member of a set of independent zero-mean unit variance Gaussian random variables. If σ_{kj} is a constant, say σ, then it is easy to show using the linearity of (2.16) that $f_w(x, y)$ is Gaussian with mean $\bar{f}_w(x, y)$ and variance $\sigma_{f_w}^2(x, y)$:

$$\sigma_{f_w}^2 = \sigma^2 \frac{2\pi d}{N}^2 \sum_{k=0}^{N-1} \sum_{j=-\infty}^{\infty} w^2(x \cos\theta_k + y \sin\theta_k - r_j) . \quad (4.4)$$

In order to reduce this variance while accurately estimating $f(x, y)$ when little or no noise is present, a different weighting function should be chosen. One such simple weighting function which has been advanced[14,15] is

$$w'(R) = Aw(R) + Bw(R + d) + Bw(R - d) , \qquad (4.5)$$

where $w(\cdots)$ is either (2.22) or (2.23). In order that $w'(R)$ accurately reconstruct $f(x, y)$ when little or no noise is present, it is necessary that $A + 2B = 1$. This constraint, plus the desire that $\sigma_{f_w}^2$ be minimized, leads to an optimal choice of A (≈ 0.4) and B (≈ 0.3). Since $B = 0$ leads to w' reducing to w, it follows that

$$\sigma_{f_w'}^2 \big|_{B = 0.3} \cong (0.15) \sigma_{f_w'}^2 \big|_{B = 0} . \qquad (4.6)$$

In other words, the noise variance of the estimated function is reduced to 15% of its previous level. This gain is achieved at the expense of a loss of accuracy in reconstructing the function. Table V presents some error estimates for reconstructing an impulse using w' (see Table II).

Trying to find a weighting function which reconstructs f as accurately as possible, i.e., both with and without noise present, is still an open question, but it appears to be extremely difficult and most likely not worth the trouble since ad hoc schemes such as (4.5) are apparently quite satisfactory, as shown in the following section.

B. An example

Figure 6 is identical with Fig. 3 except that independent zero-mean Gaussian random variables with standard deviation (0.1) have been added to each mea-

TABLE IV. Estimated error in reconstructing $f(x, y)$ in Table III (same notation as in Table II used).

Number of lasers and sensors	w in (2.22)			w in (2.23)		
	E_1	E_2	E_∞	E_1	E_2	E_∞
2	0.110	0.661	5.00	0.110	0.662	5.00
4	0.319	0.618	3.99	0.286	0.615	4.17
6	0.262	0.608	4.40	0.235	0.610	4.50
8	0.307	0.557	3.56	0.268	0.554	3.76
10	0.277	0.537	3.86	0.248	0.534	3.93
20	0.198	0.452	3.66	0.184	0.449	3.67

TABLE V. Estimated error in reconstructing an impulse using Eqs. (2.16) and (4.5) (same notation as in Table II); no noise present.

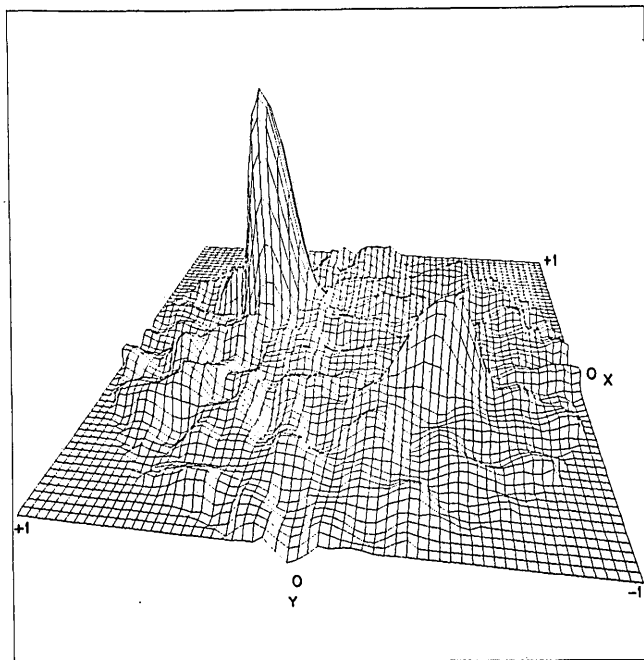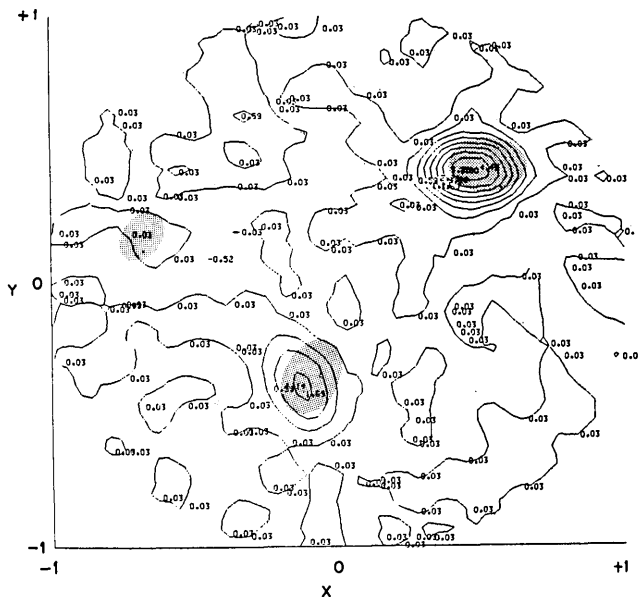| Number of lasers and sensors	w in (2.22) and (4.5)			w in (2.23) and (4.5)		
	E_1	E_2	E_∞	E_1	E_2	E_∞
2	0.318	0.417	1.00	0.312	0.417	1.00
4	0.189	0.233	0.665	0.185	0.222	0.564
6	0.0892	0.146	0.665	0.0896	0.142	0.563
8	0.0524	0.109	0.682	0.0507	0.106	0.576
10	0.0355	0.0861	0.642	0.0340	0.0848	0.545
20	0.0132	0.0487	0.749	0.0115	0.0448	0.629

FIG. 6. Reconstruction of $f(x, y)$ at 60×60 grid of points using (2.23) as a weighting pattern with pseudorandom Gaussian random variables (mean zero, standard deviation 0.1) added to each measurement, using 20 lasers and 20 sensors.

surement. Figure 7 is identical to Fig. 6, except that the weighting function in (4.5) was used. With no noise present, however, the reconstruction using (2.23) was found to be more accurate than (4.5), as shown in Table V.

C. Measurement imperfections

Besides those due to noise, measurements may also be inaccurate because (i) the lasers and sensors do not all lie in a plane $z = z_0$, (ii) the sensors and lasers are not evenly spaced, (iii) air pollutant concentration changes while the measurements are being made, and (iv) one or more of the lasers or sensors are inoperative.

Simple physical arguments show that even if the lasers and sensors are not coplanar, the basic technique may still work. Computer simulations where the measurements were offset in radius by $(0.1)ud$ and in angle by $0.1(\pi/N)r$, where u and r are independent random variables uniformly distributed on $(-\frac{1}{2}, \frac{1}{2})$, showed that (2.23) and (4.5) introduced root-mean-square absolute
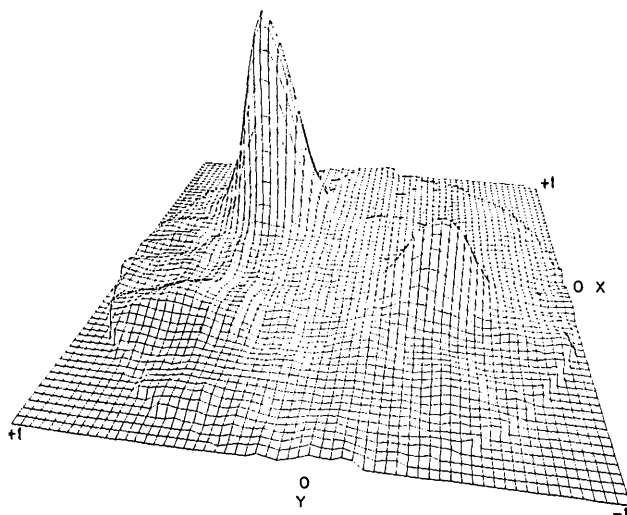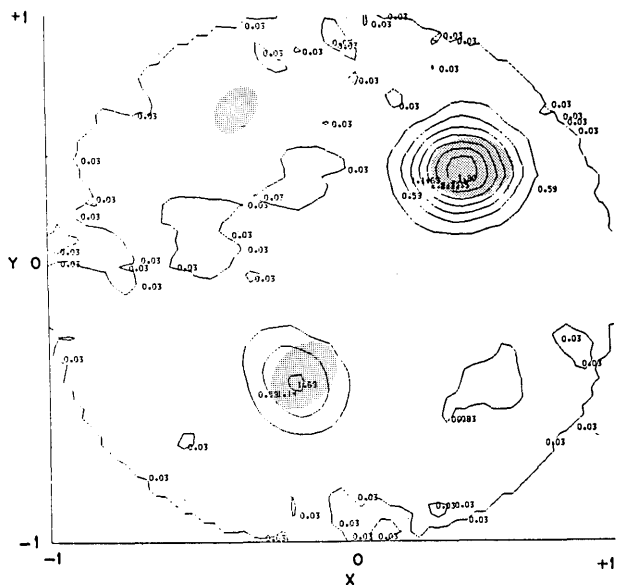

FIG. 7. Reconstruction of $f(x, y)$ at 60×60 grid of points using (2.23) and (4.5) as a weighting pattern with pseudorandom Gaussian random variables (mean zero, standard deviation 0.1) added to each measurement, using 20 lasers and 20 sensors.

errors of 10% and less, which were felt to be negligible. Computer simulations with orientations yielded results quite close to that shown in Fig. 7. Finally, if even one laser or sensor fails, the algorithm in (2.16) fails, but computer results showed some qualitative information was salvageable.

V. CONCLUDING REMARKS

It is tempting to conjecture that this method could work if only incoherent sunlight were used in conjunction with a network of electro-optical sensors, rather than using lasers. This does not appear theoretically possible, from examining radiative transfer theory with Rayleigh scattering; however, the subject is still open.

ACKNOWLEDGMENTS

[1] H. W. Hermance, "Combatting the Effects of Smog on Wire-Spring Relays," Bell Lab. Rec. 44, 48–52 (1966).

[2] H. W. Hermance, C. A. Russell, E. J. Bauer, T. F. Egan, H. V. Wadlow," Relation of Airborne Nitrate to Telephone Equipment Damage," Environ. Sci. Technol. 5, 781–785 (1971).

[3] H. H. G. Jelink, "Chain Scission of Polymers by Small Concentrations (1 to 5 ppm) of Sulfur Dioxide and Nitrogen Dioxide, Respectively, in the Presence of Air and Near Ultraviolet Radiation," J. Air Pollut. Control Assoc. 20, 672–674 (1970).

[4] T. E. Graedel, "The Atmospheric Environment Encountered by Electrical Components," in Proceedings of the 19th Annual Holm Seminar on Electric Contact Phonomena, Chicago, Ill. (1973) (unpublished).

[5] D. E. Gower, "Air Monitoring Methods and Instrumentation Performance Experiences in the New York State Continuous Air Monitoring System," Tech. Rep. BA QS-41, N. Y. Dept. Environmental Conservation, May 1973 (unpublished).

[6] N. J. Dept. Environmental Protection, "The New Jersey Continuous Air Monitoring Network," Tech Bulletin A-72-1, July 1972 (unpublished).

[7] D. E. Gower "New York State Photochemical Oxidant Studies," Tech. Rep. BA QS-42, N. Y. Dept. Environmental Conservation, Jan. 1973 (unpublished).

[8] R. T. H. Collis, "Lidar," Appl. Opt. 9, 1782–1788 (1970).

[9] R. T. H. Collis and E. V. Uthe, "Mie Scattering Techniques for Air Pollution Measurement with Lasers," Opto-electronics 4, 87–99 (1972).

[10] H. Inaba and T. Kobayasi, "Laser Raman Radar," Opto-electronics 4, 101–123 (1972).

[11] P. L. Hanst, in Advances in Environmental Science and Technology, edited by J. N. Pitts and R. L. Metcalf (Wiley, New York, 1971), pp. 91–213.

[12] R. N. Bracewell and A. C. Riddle, "Inversion of Fan-Beam Scans in Radio Astronomy," Astrophys. J. 150, 427–434 (1967).

[13] G. N. Ramachandran and A. V. Lakshminarayanan, "Three Dimensional Reconstruction from Radiographs and Electron Micrographs: Application of Convolutions Instead of Fourier Transforms," Proc. Nat. Acad. Sci. USA 68, 2236–2240 (1971).

[14] L. A. Shepp and B. F. Logan, "Reconstructing Interior Head Tissue from X-ray Transmissions," IEEE Trans. Nucl. Sci. NS-21, 228–236 (1974).

[15] L. A. Shepp and B. F. Logan, "The Fourier Reconstruction of a Head Section," IEEE Trans. Nucl. Sci. (to be published).

[16] J. G. Schneeman, Industrial X-ray Interpretation (Intex, Evanston, Illinois, 1968).

[17] J. A. Hodgeson, W. A. McClenny and P. L. Hanst, "Air Pollution Monitoring by Advanced Spectroscopic Techniques," Science 182, 248–258 (1973).

[18] E. D. Hinkley, "Tunable Infra-red Lasers and Their Applications to Air Pollution Measurements," Opto-electronics 4, 69–82 (1972).

[19] E. D. Hinkley and A. R. Calawa, in "Diode Lasers for Pollutant Monitoring," in Analysis Methods Applied to Air Pollution Measurements, edited by R. K. Stevens and W. F. Herget (Ann Arbor Science, Ann Arbor, Michigan, 1977).

[20] K. W. Rothe, V. Brinkman, and H. Walther, "Applications of Tunable Dye Lasers to Air Pollution Detection: Measurements of Atmospheric NO_2 Concentrations by Differential Absorption," App. Phys. 3, 115–119 (1974).

[21] W. B. Grant, R. D. Hake, Jr., E. M. Liston, R. C. Robbins, and E. K. Proctor, Jr., "Calibrated Remote Measurement of NO_2 Using the Differential - Absorption Backscatter Technique," Appl. Phys. Lett. 24, 550–552, (1974).

[22] K. W. Rothe, V. Brinkman, and H. Walther, "Remote Measurement of NO_2 Emission From A Chemical Factory by the Differential Absorption Technique," Appl. Phys. 4, 181–182, (1974).

[23] W. B. Grant and R. D. Hake, Jr., "Calibrated Remote Measurements of SO_2 and O_3 Using Atmospheric Backscatter," J. Appl. Phys. 46, 3019–3023 (1975).

[24] E. R. Murray, R. D. Hake, Jr., J. E. Van Der Laan, and J. G. Hawley, "Atmospheric Water Vapor Measurements with an Infrared (10-μm) Differential Absorption Lidar System," Appl. Phys. Lett. 28, 542–543 (1976).

[25] S. Chandrasekhar, Radiative Transfer (Dover, New York, 1960).

[26] R. S. Lawrence and J. W. Strohbehn, "A Survey of Clear-Air Propagation Effects Relevant to Optical Communications," Proc. IEEE 58, 1523–1546 (1970).

[27] H. Melchior, "Sensitive High Speed Photodetectors for the Demodulation of Visible and Near Infrared Light," J. Lumin. 7, 390–414 (1973).

[28] W. Kohler and G. Papanicolaou, "Power Statistics for Wave Propagation in One Dimension and Comparison with Radiative Transport Theory," J. Math. Phys. 14, 1733–1745 (1973).

[29] W. Kohler and G. Papanicolaou, "Power Statistics for Wave Propagation in One Dimension and Comparison with Radiative Transport Theory, II," J. Math. Phys. 15, 2186–2197 (1974).

[30] B. F. Logan and L. A. Shepp, "Reconstructing Pictures from Projections," (unpublished report).

[31] See also, I. M. Gellfand, M. I. Graev, and N. Ya Vilenkin, Generalized Functions, Volume 5: Integral Geometry and Representation Theory (Academic, New York, 1966), Chaps. 1 and 2.

[32] L. R. Rabiner and R. W. Schafer, "On the Behavior of Minimax FIR Digital Hilbert Transformers," Bell Syst. Tech. J. 53, 363–390 (1974).

[33] L. R. Rabiner and R. W. Schafer, "On the Behavior of Minimax Relative Error FIR Digital Differentiators," Bell Syst. Tech. J. 53, 333–361 (1974).

[34] R. M. Mersereau and A. Oppenheim, "Digital Reconstruction of Multi-Dimensional Signals from Their Projections," (unpublished).

[35] P. Gilbert, "Iterative Methods for the Three-Dimensional Reconstruction of an Object from Projections," J. Theor. Biol. 36, 105–117 (1972).

[36] R. Gordon, R. Bender and G. T. Herman, "Algebraic Reconstruction Techniques (ART) for Three Dimensional Electron Microscopy and X-ray Photography," J. Theor. Biol. 29, 471–481 (1970).